Imprinting Spatial Helicity Structure of Vector Vortex Beam on Spin Texture in Semiconductors

Jun Ishihara[1,*], Takachika Mori,[1] Takuya Suzuki,[1] Sota Sato,[2] Ken Morita,[2] Makoto Kohda,[3]
Yuzo Ohno,[4] and Kensuke Miyajima[1]

[1]*Department of Applied Physics, Tokyo University of Science, Tokyo 125-8585, Japan*
[2]*Graduate School of Electrical and Electronic Engineering, Chiba University, Chiba 263-8522, Japan*
[3]*Department of Materials Science, Tohoku University, Sendai 980-8579, Japan*
[4]*Graduate School of Pure and Applied Sciences, University of Tsukuba, Tsukuba 305-8573, Japan*

We present the transfer of the spatially variant polarization of topologically structured light to the spatial spin texture in a semiconductor quantum well. The electron spin texture, which is a circular pattern with repeating spin-up and spin-down states whose repetition rate is determined by the topological charge, is directly excited by a vector vortex beam with a spatial helicity structure. The generated spin texture efficiently evolves into a helical spin wave pattern owing to the spin-orbit effective magnetic fields in the persistent spin helix state by controlling the spatial wave number of the excited spin mode. By tuning the repetition length and azimuthal angle, we simultaneously generate helical spin waves with opposite phases by a single beam.

Spatial structures have attracted considerable attention, because their spatial modes offer a new information basis, as represented by space division multiplexing in optical communications. Topologically structured light has unique properties, such as a doughnut-shaped intensity profile, orbital angular momentum (OAM) originating from a spatial phase structure, and spatially variant polarization. Its applications include superresolution microscopy using doughnut-shaped light patterns [1,2], fabrication of chirality-dependent helical nanoneedles using an optical vortex [3,4], and optically induced rotational motion of nanoparticles by OAM [5,6]. Structured light with spatially variant polarization, such as azimuthal and radial beams, is a vector beam with nonseparable spatial and polarization degrees of freedom. This coupled spatial-polarization mode improves optical communication and optical metrology [7–11].

The spatial structures of spins in semiconductors have also drawn attention recently. A persistent spin helix (PSH), a helical spin texture in space, emerges when Rashba-type [12] and Dresselhaus-type [13] spin-orbit (SO) interactions are tuned to equal strengths in a (001)-grown quantum well (QW) with a zinc blende structure [14–16]. In the PSH state, the spatial spin texture is protected from dephasing caused by spin-independent scattering, because momentum-dependent SO effective magnetic fields are unidirectional and have an exact SU(2) symmetry. PSH can be applied not only in semiconductor-based spintronic devices using long-lived spin states, but also in devices using spatial spin modes. Studies have reported direct observations of the PSH texture [17–23], modulation of PSH

frequencies by gate voltages [18,24], and long-distance transport of the PSH by drift currents [25–28].

Semiconductors have an excellent response to light, and spin-polarized electrons can be generated in semiconductors by polarized light following optical selection rules. In addition to the optical generation and detection of spin populations, the coherent transfer of arbitrary light polarization to electron spins and the direct readout of coherent spin states have been demonstrated [29,30]. Almost all previous studies on optical spin injection have used homogeneously polarized beams, and pioneering studies on spatially structured light have demonstrated the generation of stripe-patterned polarized light created by the superposition of two homogeneously polarized beams and spin excitation by such light [16,31,32]. Vector vortex beams (VVBs) have a spatial helicity structure arising from the OAM of light, which does not exist in the Gaussian beam and the stripe-patterned polarized light described above. The use of VVBs is expected to generate novel spin textures with topological structures, thereby facilitating access to spatial spin textures and information conversion between topologically structured light and spin textures. Herein, we demonstrate the imprinting of spatial helicity structure of a VVB on the spin texture of electrons in a semiconductor QW. A spatially periodic structure of the spin state is directly generated by the VVB. In this structure, the spin-up and spin-down states are repeated in a circular pattern, and the structure period varies with the topological charge of the VVB. The excitation of the periodic spin texture by the VVB corresponds to the excitation of a specific spatial spin wave mode. This is

in contrast to spin excitation by a conventional homogeneously polarized Gaussian beam, which excites various spin wave modes simultaneously. The spatiotemporal dynamics of the spin texture reveals that the excited spin texture rapidly evolves into a PSH texture through the matching of the spatial spin mode excited by the VVB with the eigenmode of the helical spin wave of PSH induced by the SO effective magnetic field. We also show that two helical spin waves with opposite phases can be produced by a single VVB.

A VVB is generated from a homogeneously polarized beam. A linearly polarized beam is converted into an azimuthal beam by a vortex half-wave plate, whose fast axis rotates continuously in space while having a constant retardance of π. Subsequently, the beam passes through a quarter-wave plate, and a spatial pattern of polarization is obtained. The polarization of the VVB is expressed using the Jones vector as

$$\mathbf{A}_{QWP}\mathbf{A}_{VHWP}\mathbf{J}_V$$
$$= \frac{1}{\sqrt{2}}\begin{pmatrix} 1 & i \\ i & 1 \end{pmatrix}\begin{pmatrix} \cos(l\phi) & -\sin(l\phi) \\ \sin(l\phi) & \cos(l\phi) \end{pmatrix}\begin{pmatrix} 0 \\ 1 \end{pmatrix}$$
$$= \frac{i}{\sqrt{2}}e^{il\phi}\begin{pmatrix} 1 \\ -ie^{-i2l\phi} \end{pmatrix}, \tag{1}$$

where $\mathbf{A}_{QWP}$ and $\mathbf{A}_{VHWP}$ are the Jones matrices of a quarter-wave plate and vortex half-wave plate, respectively, and $\mathbf{J}_V$ is the initial linear polarization. The phase varies spatially with the azimuthal angle ϕ, as represented by $e^{il\phi}$, thereby forming a vortex beam that carries an OAM determined by the topological charge l. The spatial distribution of polarization forms a periodic structure of helicity, where left- and right-circularly polarized light is repeated in a circular pattern, as shown in Figs. 1(a) and 1(b). The VVB expressed by Eq. (1), as well as an optical vortex and the azimuthal beam, is also a polarization state that can be described by a higher-order Poincaré sphere [33,34], which is an extension of the Poincaré sphere representing the circular polarization state. When the light polarization of the VVB is coherently transferred to the electron spins, the spin states are expected to have an azimuthal angle-dependent spatial structure, as shown in Figs. 1(c) and 1(d) [34]. The arrows and the blue and red shading in Figs. 1(c) and 1(d) represent the direction of spin polarization and the out-of-plane spin component, respectively.

The imprinting of spatial helicity structure of a VVB on the spin texture of electrons is performed using a one-sided modulation-doped 20 nm GaAs/AlGaAs QW. The time evolution of the spin distribution is measured by time-resolved (TR), spatially resolved magneto-optical Kerr rotation (KR). The polarized electron spins are optically excited by the pump beam following the optical selection rule, and the out-of-plane spin component is detected as a KR signal of the linearly polarized probe beam. Optical measurements are performed at 7.5 K using a cryostat with
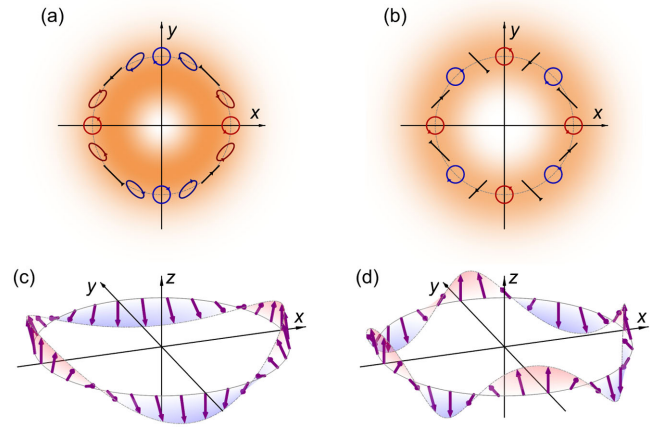

FIG. 1. Sketch of imprinting of polarization distribution by VVB on spin texture in a semiconductor QW. Azimuthal angle dependence of polarization of VVB with (a) $l = 1$ and (b) $l = 2$. (c),(d) Spatial spin structures photoexcited by VVB shown in (a) and (b) following optical selection rules. The arrows represent the polarization directions in coherent transcription, and the colors represent the spin z component.

optical access (see Supplemental Material [35] for details on the sample structure and TRKR microscopy).

Figures 2(a)–2(c) show KR maps corresponding to the spin distribution $s_z(x, y)$ immediately after spin excitation under the different pump beams. Electron spins excited by a homogeneously circularly polarized Gaussian beam are distributed around the spatial origin at $t = 19$ ps and are in the spin-up state [Fig. 2(a)]. By contrast, when the spins are excited using the VVB [Eq. (1), with $l = 1$], a twofold symmetric structure of the spin state is observed at $t = 10$ ps, as shown in Fig. 2(b); in this structure, the spin-up and spin-down states are repeated in a circular pattern. Since the VVB has a doughnut-shaped intensity profile in space originating from a topological singularity, spins are not excited into the spatial origin corresponding to the dark spot. The observed spin texture with a twofold symmetric structure indicates the presence of the spin configuration shown in Fig. 1(c) and proves that the polarization pattern of the VVB is imprinted on the spatial
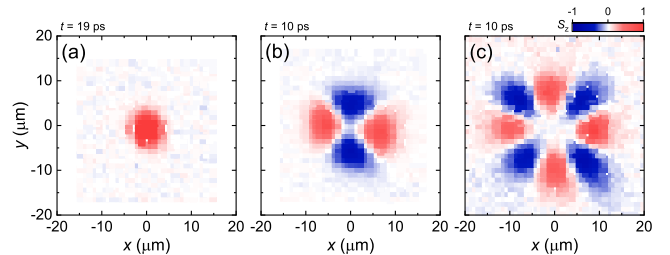

FIG. 2. KR maps corresponding to spatial spin distribution $s_z(x, y)$. (a) $s_z(x, y)$ at $t = 19$ ps excited by a homogeneously polarized beam. (b) $s_z(x, y)$ at $t = 10$ ps excited by a VVB with $l = 1$. (c) $s_z(x, y)$ at $t = 10$ ps excited by a VVB with $l = 2$.
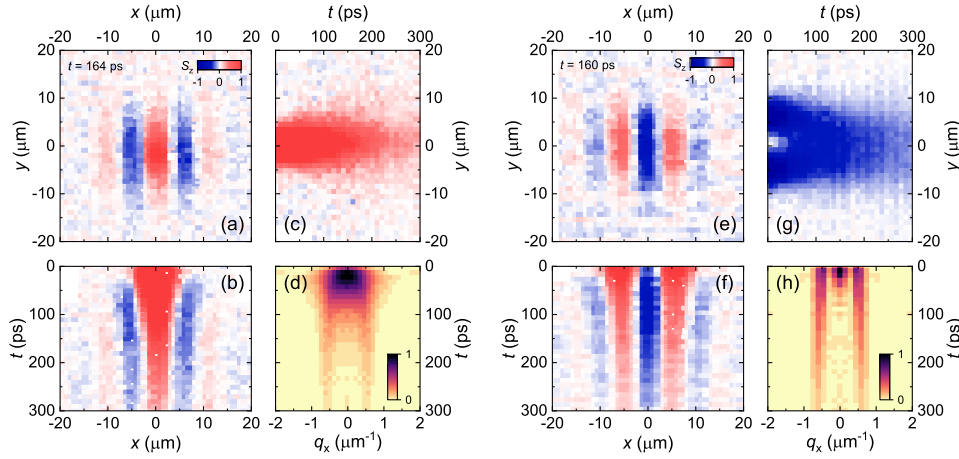
FIG. 3. (a) Spatial spin distribution $s_z(x, y)$ at $t = 164$ ps. (b) Spatiotemporal map of x direction $s_z(x, 0, t)$. (c) Spatiotemporal map of y direction $s_z(0, y, t)$. (d) Time evolution of spin wave-mode distribution $A(q_x, t)$, obtained by frequency analysis of (b) under homogeneously polarized beam spin excitation. (e) $s_z(x, y)$ at $t = 160$ ps, (f) $s_z(x, 0, t)$, (g) $s_z(0, y, t)$, and (h) $A(q_x, t)$ obtained from (f) under VVB spin excitation.

structure of the electron spin states in the semiconductor. Other spin textures can be easily generated using the VVB with different topological charges l, since the repetition rate of helicity varies with l, as shown in Eq. (1). Figure 2(c) shows the spin distribution at $t = 10$ ps excited by the VVB with $l = 2$. The spatial period of the helicity of the excitation beam is half of that with $l = 1$. Hence, the photoexcited spin texture has a fourfold symmetric structure, unlike the twofold symmetric spin texture excited by the VVB with $l = 1$. In addition, the dark spot without spin excitation enlarges due to the increase in the topological charge. Thus, the periodic helicity structure of the VVB enables the direct excitation of complex spin textures by a single beam.

Figure 3(a) shows $s_z(x, y)$ at $t = 164$ ps under homogeneous spin excitation [Fig. 2(a)]. The observed spin texture exhibits a striped pattern, with repeated spin-up and spin-down states along the x direction. Figures 3(b) and 3(c) show the time evolution of the spin distribution along the x and y directions, corresponding to $s_z(x, y = 0, t)$ and $s_z(x = 0, y, t)$, respectively. The electron spins diffuse in the QW plane from the initial spin distribution and precess with momentum-dependent SO effective magnetic fields with t. The spins moving along the x direction precess and form the helical spin pattern by the SO effective magnetic fields with time evolution, whereas the spins moving along the y direction diffuse without spin precession. Under the PSH condition in a (001) QW, where the Rashba parameter α and Dresselhaus parameter $\tilde{\beta}$ are balanced, the SO effective magnetic fields acting on moving electron spins are uniaxially oriented with the SU(2) symmetry [35]. This leads to the formation of a PSH texture with helical spin stripes. The observed spin stripe pattern suggests that the SO effective magnetic field induced by the studied QW structure is close to the PSH state. The helical spin

wavelength, which corresponds to the period of the spin stripe pattern, converges to the eigenvalue of the PSH state with t. According to the residual helical spin mode at $t = 300$ ps, as shown in Fig. 3(b), the spin precession length λ_{SO} is 11.0 ± 0.3 μm. The SO parameters are estimated as $\alpha = -1.76$ meV Å and $\tilde{\beta} = 1.44$ meV Å, and their ratio is $|\alpha/\tilde{\beta}| \sim 1.2$ [35].

The electron spins excited into the twofold symmetric spin texture by the VVB also diffuse and undergo the SO effective magnetic fields. Figure 3(e) shows the spin distribution $s_z(x, y)$ at $t = 160$ ps, which is the time elapsed from the spin distribution in Fig. 2(b). The distance between the excited spin-up states in Fig. 2(b) is intentionally set to λ_{SO} by adjusting the beam spot size. The dark spot of the spins at the spatial origin is filled by the inflow of electron spins. Moreover, the spin texture becomes a striped pattern, as in the case of spin excitation by the homogeneously polarized beam. Figures 3(f) and 3(g) show $s_z(x, 0, t)$ and $s_z(0, y, t)$ in the case of the VVB spin excitation. The spin distribution in the x direction broadens with t, forming a helical spin wave. In the y direction, the spin distribution broadens in the spin-down state without spin rotation, because the SO field acting on the electron spins moving along the y direction is canceled out. As shown in Fig. 3(f), the helical spin wave converges to the spin wave with the intrinsic spin precession length of PSH λ_{SO}, but its formation is faster than that in the case shown in Fig. 3(b). The difference in the formation time of PSH modes between homogeneously polarized beam and VVB spin excitation is caused by the wave number distributions of the spin waves in the initial spin distribution. Figures 3 (d) and 3(h) show the time evolution of the wave-mode distribution in the x direction, analyzed by the fast Fourier transformation in Figs. 3(b) and 3(f), respectively. The initial spin state with Gaussian distribution excited by the

homogeneously polarized beam includes various spin wave components with different wave numbers. Thus, the wave-mode distribution also has the Gaussian distribution in the wave number space, as shown in Fig. 3(d). As the spin waves except the long-lived spin wave of the PSH mode of $q_{PSH} = 0.6 \ \mu m^{-1}$ are relaxed, the helical spin wave with the eigenvalue of the spin precession length of the PSH state remains in real space over time. The initial spin distribution has a periodic structure in the case of VVB excitation, unlike that in the case of homogeneous spin excitation. When the distance between spin-up states is consistent with the spin precession length of the PSH, the dominant spin wave mode is already the PSH mode in the wave number space at the time of spin excitation, as shown in Fig. 3(h). That is, the eigenwave of the PSH state is directly excited by the VVB. Consequently, the helical spin wave of the PSH emerges in real space faster than that excited by the homogeneous polarized beam. The relaxation times of the PSH mode extracted from the time evolution of the amplitude of the spin wave modes at $q_x = q_{PSH} = 0.6 \ \mu m^{-1}$ of VVB and homogeneous beam excitation are 189 ± 4 and 158 ± 5 ps, respectively [35]. The difference is small, because the dephasing of the PSH mode, determined by the balance between α and $\tilde{\beta}$, is independent of the polarization distribution of the excitation light.

As shown above, VVBs can imprint their structured polarization distributions on electron spins in semiconductor QWs as spatial structures with specific wave modes. For the efficient generation of the helical spin texture, the excited spin mode should match the eigenmode of the spin wave in the PSH. Figure 4(a) shows $s_z(x, y)$ at $t = 10$ ps excited by a $\pi/4$-rotated VVB with $l = 1$ by rotating the optical axis of the retarder for VVB generation. The excited spin texture is rotated by $\pi/4$ relative to that in Fig. 2(b), but its size is the same. The periodic structure consists of spin-down and spin-up states along the positive x direction, and its phase is inverted between positive and negative y values. The rotated spin texture is diluted and destroyed over time, as shown in Fig. 4(b), although the PSH texture is clearly observed in the case of the initial spin texture shown in Fig. 2(b). For the $\pi/4$-rotated spin texture, because the distance between the spin-up and spin-down states parallel to the spin stripe direction becomes longer than half the PSH length, the excited spin mode does not match the eigenmode of the PSH texture, thereby disturbing the formation of the spin texture in real space. Figure 4(c) shows $s_z(x, y)$ at $t = 10$ ps with a smaller spot size than that in Fig. 4(a). The distance between the excited spin-up and spin-down states parallel to the x axis is approximately 5 μm, which is half the PSH length. The spin distribution evolves with time into a spin texture with spin wave structures with opposite phases in positive and negative y, as shown in Fig. 4(d). Figures 4(e) and 4(f) show the wave-mode distributions at different t values
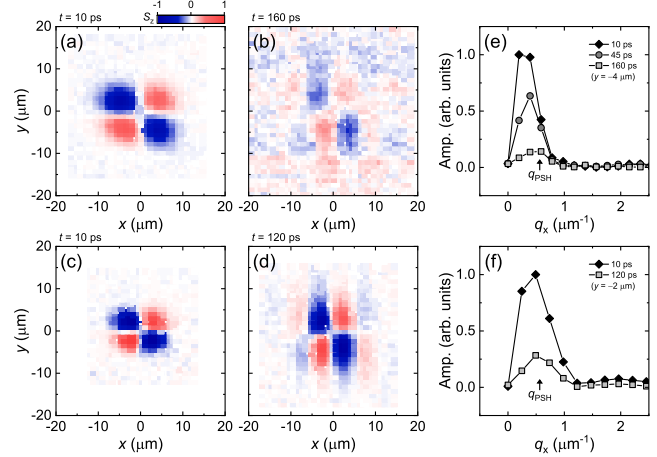

FIG. 4. Spatial spin distribution excited by $\pi/4$-rotated VVB with $l = 1$. $s_z(x, y)$ at (a) $t = 10$ ps and (b) $t = 160$ ps under large-spot spin excitation. $s_z(x, y)$ at (c) $t = 10$ ps and (d) $t = 120$ ps under small-spot spin excitation. Spin wave mode distribution in x direction at different t under (e) large-spot and (f) small-spot excitation.

under large-spot [Fig. 4(a)] and small-spot [Fig. 4(c)] excitation, respectively. For large-spot spin excitation, the dominant spin wave mode at the time of photoexcitation ($t = 10$ ps) is not the eigenmode of the PSH q_{PSH}. Subsequently, the initial spin wave mode decays, and the dominant wave modes shift toward the eigenvalue of the PSH with increasing time ($t = 45$ and 160 ps). By contrast, for small-spot spin excitation, the dominant spin wave modes do not change with time relative to the initial spin distribution. Hence, the spatial spin mode excited by the small-spot VVB is consistent with q_{PSH}. Consequently, the decrease in the spin wave mode is suppressed, and two helical spin patterns with opposite phases are clearly observed in real space with electron spin diffusion. Therefore, a new spin texture with two helical spin waves having opposite phases can be produced by a single VVB tuning a proper helicity period and azimuthal angle with respect to the helical spin stripe by only adjusting the spot size and angle of the phase plate; the use of a conventional homogeneously polarized beam cannot accomplish this process.

In conclusion, we directly generate electron spin textures by imprinting the polarization distribution of topologically structured light. The VVB imprints its periodic helicity structure arising from the OAM of light on the spatial pattern of electron spin states. The spin texture with azimuthal angle-dependent spin orientation is excited, and its rotation frequency is proportional to the topological charge. The excitation of the periodic spin texture by the VVB corresponds to the excitation of a specific spatial spin wave mode. Matching the excited spin mode with the eigenmode of the long-lived spin wave of the PSH, the formation of the PSH texture in real space is accelerated, because the extra spin wave modes that prevent the

formation of the PSH texture are not excited. We also show that a discriminative spin texture, such as the presented helical spin waves with opposite phases, can be produced even from a single beam by using a combination of helicity patterns of structured light and momentum-dependent SO effective magnetic fields. Our findings are valuable for the preparation and control of arbitrary spin textures in semiconductors and are of great importance for high-order quantum media conversion and spintronic applications using spin textures.

---

[*]j.ishihara@rs.tus.ac.jp

[1] S. W. Hell and J. Wichmann, Opt. Lett. **19**, 780 (1994).

[2] K. I. Willig, B. Harke, R. Medda, and S. W. Hell, Nat. Methods **4**, 915 (2007).

[3] K. Toyoda, K. Miyamoto, N. Aoki, R. Morita, and T. Omatsu, Nano Lett. **12**, 3645 (2012).

[4] K. Toyoda, F. Takahashi, S. Takizawa, Y. Tokizane, K. Miyamoto, R. Morita, and T. Omatsu, Phys. Rev. Lett. **110**, 143603 (2013).

[5] A. T. O'Neil, I. MacVicar, L. Allen, and M. J. Padgett, Phys. Rev. Lett. **88**, 053601 (2002).

[6] J. E. Curtis and D. G. Grier, Phys. Rev. Lett. **90**, 133901 (2003).

[7] B. Ndagano, I. Nape, M. A. Cox, C. Rosales-Guzman, and A. Forbes, J. Lightwave Technol. **36**, 292 (2018).

[8] Y. Zhao and J. Wang, Opt. Lett. **40**, 4843 (2015).

[9] G. Milione, M. P. J. Lavery, H. Huang, Y. Ren, G. Xie, T. A. Nguyen, E. Karimi, L. Marrucci, D. A. Nolan, R. R. Alfano, and A. E. Willner, Opt. Lett. **40**, 1980 (2015).

[10] S. Berg-Johansen, F. Töppel, B. Stiller, P. Banzer, M. Ornigotti, E. Giacobino, G. Leuchs, A. Aiello, and C. Marquardt, Optica **2**, 864 (2015).

[11] X.-B. Hu, B. Zhao, Z.-H. Zhu, W. Gao, and C. Rosales-Guzmán, Opt. Lett. **44**, 3070 (2019).

[12] E. I. Rashba, Sov. Phys. Solid State **2**, 1109 (1960).

[13] G. Dresselhaus, Phys. Rev. **100**, 580 (1955).

[14] J. Schliemann and D. Loss, Phys. Rev. B **68**, 165311 (2003).

[15] B. A. Bernevig, J. Orenstein, and S. C. Zhang, Phys. Rev. Lett. **97**, 236601 (2006).

[16] J. D. Koralek, C. P. Weber, J. Orenstein, B. a. Bernevig, S.-C. Zhang, S. Mack, and D. D. Awschalom, Nature (London) **458**, 610 (2009).

[17] M. P. Walser, C. Reichl, W. Wegscheider, and G. Salis, Nat. Phys. **8**, 757 (2012).

[18] J. Ishihara, Y. Ohno, and H. Ohno, Appl. Phys. Express **7**, 013001 (2013).

[19] J. Ishihara, Y. Ohno, and H. Ohno, Jpn. J. Appl. Phys. **53**, 04EM04 (2014).

[20] P. Altmann, M. P. Walser, C. Reichl, W. Wegscheider, and G. Salis, Phys. Rev. B **90**, 201306(R) (2014).

[21] G. Salis, M. P. Walser, P. Altmann, C. Reichl, and W. Wegscheider, Phys. Rev. B **89**, 045304 (2014).

[22] J. Ishihara, T. Suzuki, G. Kitazawa, T. Mori, Y. Ohno, and K. Miyajima, Phys. Rev. B **105**, 144412 (2022).

[23] F. Passmann, S. Anghel, T. Tischler, A. V. Poshakinskiy, S. A. Tarasenko, G. Karczewski, T. Wojtowicz, A. D. Bristow, and M. Betz, Phys. Rev. B **97**, 201413(R) (2018).

[24] M. Kohda, V. Lechner, Y. Kunihashi, T. Dollinger, P. Olbrich, C. Schönhuber, I. Caspers, V. V. Bel'kov, L. E. Golub, D. Weiss, K. Richter, J. Nitta, and S. D. Ganichev, Phys. Rev. B **86**, 081306(R) (2012).

[25] Y. Kunihashi, H. Sanada, H. Gotoh, K. Onomitsu, M. Kohda, J. Nitta, and T. Sogawa, Nat. Commun. **7**, 10722 (2016).

[26] P. Altmann, F. G. G. Hernandez, G. J. Ferreira, M. Kohda, C. Reichl, W. Wegscheider, and G. Salis, Phys. Rev. Lett. **116**, 196802 (2016).

[27] S. Anghel, F. Passmann, A. Singh, C. Ruppert, A. V. Poshakinskiy, S. A. Tarasenko, J. N. Moore, G. Yusa, T. Mano, T. Noda, X. Li, A. D. Bristow, and M. Betz, Phys. Rev. B **97**, 125410 (2018).

[28] S. Anghel, F. Passmann, K. J. Schiller, J. N. Moore, G. Yusa, T. Mano, T. Noda, M. Betz, and A. D. Bristow, Phys. Rev. B **101**, 155414 (2020).

[29] H. Kosaka, H. Shigyou, Y. Mitsumori, Y. Rikitake, H. Imamura, T. Kutsuwa, K. Arai, and K. Edamatsu, Phys. Rev. Lett. **100**, 096602 (2008).

[30] H. Kosaka, T. Inagaki, Y. Rikitake, H. Imamura, Y. Mitsumori, and K. Edamatsu, Nature (London) **457**, 702 (2009).

[31] A. R. Cameron, P. Riblet, and A. Miller, Phys. Rev. Lett. **76**, 4793 (1996).

[32] C. P. Weber, J. Orenstein, B. A. Bernevig, S.-C. Zhang, J. Stephens, and D. D. Awshalom, Phys. Rev. Lett. **98**, 076604 (2007).

[33] Z.-C. Ren, L.-J. Kong, S.-M. Li, S.-X. Qian, Y. Li, C. Tu, and H.-T. Wang, Opt. Express **23**, 26586 (2015).

[34] S. Sato, T. Matsumoto, Y. Nakano, J. Ishihara, K. Miyamoto, T. Omatsu, and K. Morita, arXiv:2301.08024.

[35] See Supplemental Material at http://link.aps.org/supplemental/10.1103/PhysRevLett.130.126701 for details on the sample structure, TRKR microscopy, SO effective magnetic fields in the PSH state, the estimation of SO parameters, and the lifetime of the helical spin mode, which includes Ref. [36].

[36] M. P. Walser, U. Siegenthaler, V. Lechner, D. Schuh, S. D. Ganichev, W. Wegscheider, and G. Salis, Phys. Rev. B **86**, 195309 (2012).